Universitat Autònoma de Barcelona

Dipòsit digital de documents de la UAB

This is the **accepted version** of the journal article:

Alba, David M.; Bouchet, Florian; Fortuny, Josep; [et al.]. «New remains of the Miocene great ape Anoiapithecus brevirostris from Abocador de Can Mata». Journal of Human Evolution, Vol. 188 (March 2024), art. 103497. DOI 10.1016/j.jhevol.2024.103497

This version is available at https://ddd.uab.cat/record/289506

under the terms of the BY-NC-ND license

Short Communication

New remains of the Miocene great ape *Anoiapithecus brevirostris* from Abocador de Can Mata

David M. Alba[a,*], Florian Bouchet[a], Josep Fortuny[a], Josep M. Robles[a], Jordi Galindo[a], Àngel H. Luján[a], Salvador Moyà-Solà[a,b,c], Clément Zanolli[d,*]

[a] *Institut Català de Paleontologia Miquel Crusafont (ICP-CERCA), Universitat Autònoma de Barcelona, c/ Columnes s/n, 08193 Cerdanyola del Vallès, Barcelona, Spain*

[b] *Institució Catalana de Recerca i Estudis Avançats (ICREA), Pg. Lluís Companys 23, 08010 Barcelona, Spain*

[c] *Unitat d'Antropologia Biològica (Dept. BABVE), Universitat Autònoma de Barcelona, 08193 Cerdanyola del Vallès, Barcelona, Spain*

[d] *Univ. Bordeaux, CNRS, MCC, PACEA, UMR 5199, F-33600 Pessac, France*

***Corresponding authors.**

E-mail addresses: david.alba@icp.cat (D.M. Alba); clement.zanolli@gmail.com (C. Zanolli).

Short Communication

New remains of the Miocene great ape *Anoiapithecus brevirostris* from Abocador de Can Mata

Keywords: Fossil primates; Hominoidea; Dryopithecinae; Middle Miocene; Spain

1. Introduction

The local stratigraphic sequence of Abocador de Can Mata (ACM; Alba et al., 2006), located in the Vallès-Penedès Basin (NE Iberian Peninsula) and spanning from ~12.6 to 11.1 Ma (Moyà-Solà et al., 2009b; Casanovas-Vilar et al., 2011, 2016a, 2016b; Alba et al., 2017, 2022), has yielded fossil hominoid remains attributed to three species: *Pierolapithecus catalaunicus* from ACM/BCV1 (12.0 Ma; Moyà-Solà et al., 2004); *Anoiapithecus brevirostris* from ACM/C3-Aj (12.0 Ma) and ACM/C1-E* (12.4–12.3 Ma; Moyà-Solà et al., 2009a; Alba et al., 2013); and *Dryopithecus fontani* from ACM/C3-Ae, ACM/C4-Ap and, tentatively, ACM/C3-Az (11.9 Ma; Moyà-Solà et al., 2009b; Alba and Moyà-Solà, 2012). Additional remains of '*Sivapithecus*' *occidentalis* (species inquirenda) have been recovered from Can Vila and ACM/BCV4 (11.9 Ma; Alba et al., 2020), being potentially attributable to either *P. catalaunicus* or *A. brevirostris*, while indeterminate dryopithecine remains have been also recovered between 11.8 and 11.1 Ma (Alba et al., 2017, 2022). Here, we describe hominoid upper teeth recovered in 2006 from locality ACM/C4-Cp, which has an estimated age of 11.9 Ma (Alba et al., 2022) and was located relatively close to, but stratigraphically 16 m below, ACM/C4-Ap (Supplementary Online Material [SOM] Fig. S1), with an estimated age difference of 70 kyr (Alba et al., 2022). The dental remains from ACM/C4-Cp were previously reported by Alba (2012) as Hominidae indet. and by Alba et al. (2017, 2022) as *A.*

brevirostris, but remained unpublished. Here we describe and figure them for the first time and provide morphological and morphometric comparisons to justify their attribution to *A. brevirostris*.

2. Materials and methods

IPS41713a–e consists of five upper teeth (Table 1) that constitute a left C^1–M^2 series from a single male adult individual (see SOM S1 and SOM Fig. S2 for further details). Dental measurements of length (MD) and breadth (BL) were taken with a digital caliper to the nearest 0.1 mm and used to compute a breadth/length index (BLI = BL / MD × 100); to measure the length of the C^1, the mesiodistal axis was defined as the maximum basal crown diameter and the labiolingual one as perpendicular to it. The comparative sample includes other Iberian dryopithecines, with emphasis on Middle Miocene taxa from the Vallès-Penedès Basin (see measurements in SOM Table S1).

The cheek teeth were µCT-scanned and segmented to generate three-dimensional (3D) surface models of the outer enamel surface (OES) and the enamel-dentine junction (EDJ)—see SOM S2.1 for details on scanning parameters and segmentation. The OES and EDJ 3D surfaces are available from MorphoSource (SOM Table S2). Two-dimensional relative enamel thickness (2DRET) was computed following standard procedures (e.g., Fortuny et al., 2021; see SOM S2.2). The incomplete preservation of the crown base precluded computing enamel thickness in 3D as well the application of alternative deformation-based methods of shape analysis (e.g., Zanolli et al., 2023). However, a 3D geometric morphometric (3DGM) analysis of EDJ shape of the M^1 was performed using (semi)landmarks (SOM Fig. S3) to assess the closest morphometric affinities of the specimen. Shape coordinates were subjected to two different statistical analyses: a canonical variate analysis (CVA) based on extant great ape genera (Zanolli et al., 2023: SOM Table S2) and a principal component analysis (PCA) based exclusively on Vallès-Penedès dryopithecines (Fortuny et al., 2021; Zanolli et al., 2023; see SOM Table S3). For additional details on shape analysis and the comparative sample, see SOM S2.3.

3. Results

3.1. Description

The upper canine The C^1 (Fig. 1a–e; Table 1) is labiolingually very compressed, more markedly so at the crown (BLI = 63%) than at the root, which is somewhat stouter, higher, and distally tilted relative to the apicobasal crown axis. The apex of the crown appears almost unworn, with a preserved labial crown height of >14.6 mm (it cannot be measured with certainty due to damage at the cervix). The crown displays a marked and deep mesiolingual sulcus that does not extend onto the root through the cervix and apically fades before reaching the crown apex. The crown curves lingually from base to apex and is thus lingually tilted. The labial crown wall is markedly convex, while the distolingual one appears basally concave due to honing against the P_3, which would have presumably maintained a sharp distal margin (although this cannot be unambiguously confirmed due to damage).

The upper premolars The P^3 (Fig. 1f, j) only shows minimal wear at the paracone apex but, due to incomplete preservation, it is not informative about occlusal proportions. The preparacrista is straighter and more mesiodistally aligned than the postparacrista, which is not continuous with the distal marginal ridge. Moderately well-developed styles can be discerned on the mesiobuccal and distobuccal corners of the crown. Two distinct transverse crests originate from the buccal aspect of the protocone and reach the lingual base of the paracone, delimiting a deep but restricted, rectangular (much broader than long) central fovea, which is well distinct from the partially preserved mesial fovea and the more spacious and deeper distal fovea. The latter shows some development of enamel wrinkling. At the mesial fovea, a moderately distinct hypoparacrista of mesiolingual direction appears to bifurcate at about its midway. The postprotocrista is curved and continuous with the distal marginal ridge.

The P^4 (Fig. 1g, l) is similarly worn but more completely preserved than the P^3 and hence enables a rough estimation of crown proportions. The crown displays a suboval occlusal contour that is slightly longer lingually than buccally and much broader than long (BLI ≈ 147%; Table 1). Although the lingual and buccal crown walls are not preserved at the crown base, it can be ascertained that the protocone is subequal in size to the paracone and that the buccal crown wall is only moderately flaring. As in the P^3, there are two transverse crests between the protocone and paracone that delimit a broader than long central fovea, although less distinct than in the P^3 because the crests are less well defined (maybe due to damage). Also, as in the P^3, an oblique (albeit less distinct) hypoparacrista divides the mesial fovea, the curved postprotocrista merges with the distal marginal ridge, and the postparacrista is more obliquely oriented than the protoparacrista and curves lingually before reaching the distal marginal ridge (although the distobuccal style is less distinct than in the P^3). Although there are some indications of enamel wrinkling, they are difficult to distinguish from damage on the OES.

The EDJ shape of the premolars (Fig. 1k, m) supports the descriptions provided above based on the OES and shows some additional details. It confirms that the postparacrista does not reach the distal marginal ridge but abruptly curves lingually before reaching it (in the P^4 merging with a short and lingually oriented secondary crest), that the two transverse crests originate from the lingual aspect of the protocone dentine horn, and that in the P^4

the distal transverse crest fades away clearly before reaching the postprotocrista. In the P^4, the oblique hypoparacrista reaches the mesial marginal ridge, completely isolating a restricted mesiobuccal fovea from the rest of the mesial fovea. Enamel wrinkling is not generally expressed at the EDJ, except for some tenuous secondary ridges.

The upper molars The M^1 (Fig. 1h, n) is only slightly worn (with no dentine exposure despite some damage at the metacone apex) and displays tenuous mesial and distal interproximal wear facets. The enamel is moderately thick (2DRET = 15.54; SOM Fig. S4; SOM Table S4). The occlusal contour is subquadrangular (slightly broader than long; BLI ≈ 110%; Table 1) and moderately distally tapering (albeit this might be attributable to the more incomplete preservation of the distobuccal crown base). There are four main cusps, the lingual ones (especially the protocone) slightly more distally located than the corresponding buccal cusps. The hypocone is well developed (subequal in size to the trigon cusps) and slightly more lingually located than the protocone. There is also a distinct but smaller protoconule (=paraconule) located mesiobuccally from the paracone, at the junction between the short and mesiobuccally oriented preprotocrista and the mesial marginal ridge. The latter is also continuous with the short preparacrista. A thick and transversely aligned hypoparacrista extends between the bases of the protoconule and the paracone, separating a fissure-like mesial fovea (mostly located on the buccal half of the crown) from the subtriangular and much more extensive deeper trigon basin. The latter is delimited distally by a straight, thick, sharp, and continuous crista obliqua, and buccally by the similarly distinct but narrower postparacrista and premetacrista, which are aligned to one another. The bases of the protocone and hypocone are separated by a deep transverse groove that extends from the buccal wall to the center of the distal fovea across the poorly-defined prehypocrista. A short, thick, and blunt transverse crista extends between the bases of the hypocone and metacone, dividing the distal fovea. The posthypocrista and postmetacrista are short, curved, and continuous with the distal marginal ridge. Very narrow cingular remnants are present mesiolingually and distolingually, while a narrow buccal cingulum was likely present between the paracone and metacone (albeit this cannot be conclusively ascertained owing to incomplete preservation). The occlusal morphology preserved by the partial M^2 (Fig. 1i, p) is entirely comparable to that of the M^1 at a larger size, except for the more conspicuous prehypocrista (even if partly interrupted by the aforementioned transverse groove) and the more abundant development of secondary enamel wrinkling at the distal fovea.

The EDJ shape of the molars (Fig. 1o, q) further confirms the descriptions provided above for the OES, including the presence of a well-developed protoconule horn tip, a distinct hypoparacrista separating the mesial from the central fovea, a continuous crista obliqua, and a hypocone-metacone transverse crest dividing the distal fovea. The prehypocrista, which is continuous and more clearly defined than at the OES level, is obliquely oriented and does not join the apex of the protocone dentine horn but the origin of the postprotocrista, where a poorly-developed secondary dentine horn can be discerned in the M^1 but not in the M^2.

3.2. Comparisons

The upper canine Among the male C^1 sample of Middle Miocene dryopithecines from the Vallès-Penedès Basin, IPS41713a (Fig. 2a) most closely resembles that of the *A. brevirostris* holotype (Fig. 2b), which displays a slightly larger but similarly slender crown with an elliptical and markedly labiolingually compressed occlusal contour (SOM Fig. S5a; SOM Table S1) and a lingually tilted apex. Besides minor size differences, these two specimens only slightly differ in the shape of the root, which is straighter in the holotype of *A. brevirostris* (forming a more abrupt angle with the crown apicobasal axis than in IPS41713a). The male C^1s of the *P. catalaunicus* holotype (Fig. 2e–f) show a similar degree of crown labiolingual compression and a lingually tilted crown apex but display somewhat larger and less labiolingually compressed crown basal dimensions (SOM Fig. S5a; SOM Table S1), a less elliptical occlusal contour (more constricted at about mid-length), and a stouter root. The male C^1s of *D. fontani* (Fig. 2d) display larger dimensions (SOM Fig. S5a; SOM Table S1), especially breadth, resulting in a much broader crown than in *A. brevirostris*, further displaying a clearly suboval instead of elliptical occlusal contour that is broadest toward the mesial side and more distally tapering than in the remaining specimens. Furthermore, in *D. fontani* the crown apex is not lingually tilted as in IPS41713a and the holotypes of *A. brevirostris* and *P. catalaunicus*.

<u>The upper premolars</u> The upper cheek teeth of IPS41713 and its M^1 OES and EDJ are compared with those of Middle Miocene dryopithecines from the Vallès-Penedès Basin in Figure 2 and SOM Figure S6, respectively, while dental size and proportions (SOM Table S1) can be ascertained from bivariate plots depicted in SOM Figure S5b–c.

The upper premolars show a similar occlusal pattern to those of other Middle Miocene dryopithecines, characterized by the presence of two transverse crests between the protocone and the paracone, although further comparisons are restricted to the P^4 due to the incomplete preservation of the P^3. The described P^4 (IPS41713b) is larger than female specimens of *A. brevirostris* and more closely resembles in size those of other male dryopithecines (SOM Fig. S5b). However, its proportions most closely approach those of the *A. brevirostris* male holotype, whereas the P^4s of *D. fontani* and especially *P. catalaunicus*—which display a more flaring buccal crown wall at the level of the paracone—are relatively broader (SOM Fig. S5b; SOM Table S1). The newly described P^4 apparently differs from those in the comparative sample because the distal transverse crest does not join the postparacrista, where it usually forms a cuspule-like thickening, but this is difficult to ascertain at the OES level due to damage.

The upper molars In dental size and proportions, the M^1 from ACM/C4-Cp resembles those of Middle Miocene dryopithecine male individuals included in the comparative sample and is larger than those of female specimens of *A. brevirostris* (SOM Fig. S5c; SOM Table S1). All these M^1s show a similar occlusal pattern at the OES and EDJ levels (Fig. 2; SOM Fig. S6), including the presence of a distinct protoconule, a small buccal cingulum between the paracone and metacone (not confidently ascertainable in IPS41713d owing to incomplete preservation), and a hypocone-metacone crest. Nevertheless, IPS41713d differs from the holotype of *P. catalaunicus* in the slightly more lingual position of the hypocone and the somewhat less inflated crests. Another possible difference refers to the orientation of the hypocone-metacone crista, which in IPS41713d is transversely oriented from the hypocone toward the metacone base, as in previously described specimens of *A. brevirostris*. By contrast, this crest is more obliquely oriented (i.e., directed toward the end of the postmetacrista) in *P. catalaunicus* and *D. fontani*. The 2DRET displayed by the M^1 from ACM/C4-Cp is higher than that of African apes and more similar to that of orangutans, more closely approaching the condition of *A. brevirostris* and *P. catalaunicus* than the thinner-enameled condition of *D. fontani* (SOM Fig. S7; Fortuny et al., 2021).

The 3DGM analyses of EDJ shape confirm that the M^1 from ACM/C4-Cp displays closest morphometric affinities with other dryopithecines from the Vallès-Penedès Basin. The CVA (Fig. 3a), which maximizes the distinction among extant great ape genera and correctly classifies 97% of original cases (93% after cross-validation; SOM Table S5), indicates that all dryopithecines occupy an intermediate position in the morphospace along the first canonical variate (CV1) but overlap with extant great apes in the second (CV2)—see SOM S3.1, SOM Table S6, and SOM Figure S8 for a more detailed description of the results. The Late Miocene *Hispanopithecus* shows moderately negative CV2 scores, while the Middle Miocene genera show slightly more positive scores along this axis. IPS41713 shows slightly less negative scores than the other analyzed dryopithecines along CV1, whereas it only overlaps with *Anoiapithecus* specimens along CV2, being approximately equidistant from the holotype of the latter species and the single specimen of *Dryopithecus*. Typicality probabilities indicate that none of the fossil specimens (including IPS41713) fit with the variation of any extant genus (SOM Table S7). The PCA focused on dryopithecines (Fig. 3b zzz), which does not distort the morphospace to maximize the variance among taxa, shows some differences between Late and Middle Miocene taxa along the first principal component (PC1) with only slight overlap, while PC2 separates *Anoiapithecus* from other taxa (see SOM S3.2 and SOM Table S8 for further details of the PCA results). Overall, the M^1 from ACM/C4-Cp appears approximately equidistant to *Hispanopithecus laietanus* and the holotypes of *A. brevirostris* and *P. catalaunicus*, and most distinctive from both *D. fontani* and *Hispanopithecus crusafonti*.

4. Discussion and conclusions

Middle and Late Miocene dryopithecines from Iberia have been variously recovered by cladistic analyses as crown hominids of uncertain affinities (Nengo et al., 2017; Gilbert et al., 2020), as stem hominids (Alba et al., 2015; Pugh, 2022), or as stem hominines (Sevim-Erol et al., 2023). Given such contradictory results (for further discussion, see Alba, 2012; Almécija et al., 2021; Urciuoli and Alba, 2023), coupled with taxonomic controversies about the distinctiveness of the Middle Miocene genera (Begun, 2009, 2015) and the scarcity of fossil great ape remains from Europe, every bit of new information is important. For example, analyses of tooth endostructural morphology of these dryopithecines (Alba et al., 2010, 2013, 2020; Fortuny et al., 2021; Zanolli et al., 2023) have supported the presence of some differences in enamel thickness and EDJ shape among Iberian dryopithecine genera, in further agreement with differences in OES (Alba and Moyà-Solà, 2012; Alba et al., 2013, 2020; Pérez de los Ríos et al., 2013) and cranial (Moyà-Solà et al., 2004, 2009a, 2009b; Pérez de los Ríos et al., 2012; Pugh et al., 2023) morphology. Nevertheless, all these analyses suffer from the problem of small sample sizes, which, coupled with their likely close phylogenetic relationships, hinder adequately evaluating intra- vs. interspecific variation.

The description and analysis of the hominoid dental remains from ACM/C4-Cp modestly enlarge the previously available upper tooth samples and reinforce previous purported differences noted among Middle Miocene dryopithecine genera from the Vallès-Penedès Basin. According to previous accounts of the dental morphology of these taxa (Alba and Moyà-Solà, 2012; Alba et al., 2013), *Anoiapithecus* would differ from *Pierolapithecus* in the less inflated cheek tooth crests, less developed enamel wrinkling, and the more lingually located hypocone in the upper molars, from *Dryopithecus* in the thicker molar enamel, and from both genera in the size and proportions of the male C^1 and the lower-crowned upper molars. The latter feature cannot be reliably measured in the newly described specimens due to incomplete preservation, and differences in enamel wrinkling are difficult to ascertain in the M^1 due to differential wear. Nevertheless, the M^1 from ACM/C4-Cp most closely resembles those attributed to *A. brevirostris* in some features, differing from *Pierolapithecus* in the less inflated crests and the more lingually located hypocone, from *Dryopithecus* in the thicker enamel, and from both genera in the more transversely aligned hypocone-metacone crest. Our 3DGM analyses of M^1 EDJ shape are not entirely conclusive, but confidently rule out an attribution to *D. fontani*. The P^4 occlusal proportions and contour further support an attribution to *A. brevirostris*, like the male C^1, which displays closest similarities in both shape (labiolingual crown compression and lingual tilt of the apex) and size to that of the *A. brevirostris* and, to a lesser extent, that of the *P. catalaunicus*, most clearly discounting an alternate attribution to *D. fontani* (which displays larger size, broader proportions, and a less lingually tilted apex). We therefore conclude that, when all available evidence from the upper teeth is taken into account, an attribution of IPS41713 *A. brevirostris* is warranted.

Acknowledgments

This article is part of R+D+I projects PID2020-117289GB-I00, PID2020-117118GB-I00, and PID2020-116908GB-I00, funded by the Agencia Estatal de Investigación of the Spanish Ministerio de Ciencia e Innovación (MCIN/AEI/10.13039/501100011033/), and has also been supported by the Generalitat de Catalunya/CERCA Programme, the Agència de Gestió d'Ajuts Universitaris i de Recerca of the Generalitat de Catalunya (2001 SGR 00620, 2001 SGR 01184, and 2001 SGR 01188), the Departament de Cultura of the Generalitat de Catalunya (CLT0009_22_000018), a Ramón y Cajal grant to J.F. (RYC2021-032857-I) financed by the Ministerio de Ciencia e Innovación (MCIN/AEI/10.13039/501100011033) and the European Union «NextGenerationEU» / PRTR, and the Beatriu de Pinós postdoctoral programme (2019 BP 00154 to À.H.L.). The µCT scan was performed at the Centro Nacional de Investigación sobre Evolución Humana (CENIEH) facilities (Burgos) with the collaboration of the CENIEH staff. We thank the staff of the Preparation & Conservation Area of the ICP for the preparation of the specimens, and Alejandro Serrano-Martínez for assistance in µCT-scanning. Finally, we acknowledge the Editor (Andrea Taylor), Associate Editor, and three anonymous reviewers for helpful comments and suggestions that helped us improve a previous version of this paper.

References

Alba, D.M., 2012. Fossil apes from the Vallès-Penedès Basin. Evol. Anthropol. 21, 254–269.

Alba, D.M., Moyà-Solà, S., 2012. On the identity of a hominoid male upper canine from the Vallès-Penedès Basin figured by Pickford (2012). Estud. Geol. 68, 149–153.

Alba, D.M., Moyà-Solà, S., Casanovas-Vilar, I., Galindo, J., Robles, J.M., Rotgers, C., Furió, M., Angelone, C., Köhler, M., Garcés, M., Cabrera, L., Almécija, S., Obradó, P., 2006. Los vertebrados fósiles del Abocador de Can Mata (els Hostalets de Pierola, l'Anoia, Cataluña), una sucesión de localidades del Aragoniense superior (MN6 y MN7+8) de la cuenca del Vallès-Penedès. Campañas 2002-2003, 2004 y 2005. Estud. Geol. 62, 295–312.

Alba, D.M., Fortuny, J., Moyà-Solà, S., 2010. Enamel thickness in Middle Miocene great apes *Anoiapithecus*, *Pierolapithecus* and *Dryopithecus*. Proc. R. Soc. B 277, 2237–2245.

Alba, D.M., Fortuny, J., Pérez de los Ríos, M., Zanolli, C., Almécija, S., Casanovas-Vilar, I., Robles, J.M., Moyà-Solà, S., 2013. New dental remains of *Anoiapithecus* and the first appearance datum of hominoids in the Iberian Peninsula. J. Hum. Evol. 65, 573–584.

Alba, D.M., Almécija, S., DeMiguel, D., Fortuny, J., Pérez de los Ríos, M., Pina, M., Robles, J.M., Moyà-Solà, S., 2015. Miocene small-bodied ape from Eurasia sheds light on hominoid evolution. Science 350, aab2625.

Alba, D.M., Casanovas-Vilar, I., Garcés, M., Robles, J.M., 2017. Ten years in the dump: An updated review of the Miocene primate-bearing localities from Abocador de Can Mata (NE Iberian Peninsula). J. Hum. Evol. 102, 12–20.

Alba, D.M., Fortuny, J., Robles, J.M., Bernardini, F., Pérez de los Ríos, M., Tuniz, C., Moyà-Solà, S., Zanolli, C., 2020. A new dryopithecine mandibular fragment from the middle Miocene of Abocador de Can Mata and the taxonomic status of '*Sivapithecus*' *occidentalis* from Can Vila (Vallès-Penedès Basin, NE Iberian Peninsula). J. Hum. Evol. 145, 102790.

Alba, D.M., Robles, J.M., Casanovas-Vilar, I., Beamud, E., Bernor, R.L., Cirilli, O., DeMiguel, D., Galindo, J., Llopart, I., Pons-Monjo, G., Sánchez, I.M., Vinuesa, V., Garcés, M., 2022. A revised (earliest Vallesian) age for the hominoid-bearing locality of Can Mata 1 based on new magnetostratigraphic and biostratigraphic data from Abocador de Can Mata (Vallès-Penedès Basin, NE Iberian Peninsula). J. Hum. Evol. 170, 103237.

Almécija, S., Hammond, A.S., Thompson, N.E., Pugh, K.D., Moyà-Solà, S., Alba, D.M., 2021. Fossil apes and human evolution. Science 372, eabb4363.

Begun, D.R., 2009. Dryopithecins, Darwin, de Bonis, and the European origin of the African apes and human clade. Geodiversitas 31, 789–816.

Begun, D.R., 2015. Fossil record of Miocene hominoids. In: Henke, W., Tattersall, I. (Eds.), Handbook of Paleoanthropology, 2nd ed. Springer, Heidelberg, pp. 1261–1332.

Casanovas-Vilar, I., Alba, D.M., Garcés, M., Robles, J.M., Moyà-Solà, S., 2011. Updated chronology for the Miocene hominoid radiation in Western Eurasia. Proc. Natl. Acad. Sci. USA 108, 5554–5559.

Casanovas-Vilar, I., Madern, A., Alba, D.M., Cabrera, L., García-Paredes, I., Van den Hoek Ostende, L.W., DeMiguel, D., Robles, J.M., Furió, M., Van Dam, J., Garcés, M., Angelone, C., Moyà-Solà, S., 2016a. The Miocene mammal record of the Vallès-Penedès Basin (Catalonia). C. R. Palevol 15, 791–812.

Casanovas-Vilar, I., Garcés, M., Van Dam, J., García-Paredes, I., Robles, J.M., Alba, D.M., 2016b. An updated biostratigraphy for the late Aragonian and the Vallesian of the Vallès-Penedès Basin (Catalonia). Geol. Acta 14, 195–217.

Fortuny, J., Zanolli, C., Bernardini, F., Tuniz, C., Alba, D.M., 2021. Dryopithecine palaeobiodiversity in the Iberian Miocene revisited on the basis of molar endostructural morphology. Palaeontology 64, 531–554.

Gilbert, C.C., Ortiz, A., Pugh, K.D., Campisano, C.J., Patel, B.A., Singh, N.P., Fleage, J.G., Patnaik, R., 2020. New middle Miocene ape (Primates: Hylobatidae) from Ramnagar, India fills major gaps in the hominoid fossil record. Proc. R. Soc. B 287, 20201655.

Moyà-Solà, S., Köhler, M., Alba, D.M., Casanovas-Vilar, I., Galindo, J., 2004. *Pierolapithecus catalaunicus*, a new Middle Miocene great ape from Spain. Science 306, 1339–1344.

Moyà-Solà, S., Alba, D.M., Almécija, S., Casanovas-Vilar, I., Köhler, M., De Esteban-Trivigno, S., Robles, J.M., Galindo, J., Fortuny, J., 2009a. A unique Middle Miocene European hominoid and the origins of the great ape and human clade. Proc. Natl. Acad. Sci. USA 106, 9601–9606.

Moyà-Solà, S., Köhler, M., Alba, D.M., Casanovas-Vilar, I., Galindo, J., Robles, J.M., Cabrera, L., Garcés, M., Almécija, S., Beamud, E., 2009b. First partial face and upper dentition of the Middle Miocene hominoid *Dryopithecus fontani* from Abocador de Can Mata (Vallès-Penedès Basin, Catalonia, NE Spain): Taxonomic and phylogenetic implications. Am. J. Phys. Anthropol. 139, 126–145.

Nengo, I., Tafforeau, P., Gilbert, C.C., Fleagle, J.G., Miller, E.R., Feibel, C., Fox, D.L., Feinberg, J., Pugh, K.D., Berruyer, C., Mana, S., Engle, Z., Spoor, F., 2017. New infant cranium from the African Miocene sheds light on ape evolution. Nature 548, 169–174.

Pérez de los Ríos, M., Moyà-Solà, S., Alba, D.M., 2012. The nasal and paranasal architecture of the Middle Miocene ape *Pierolapithecus catalaunicus* (Primates: Hominidae): Phylogenetic implications. J. Hum. Evol. 63, 497–506.

Pickford, M., 2012. Hominoids from Neuhausen and other Bohnerz localities, Swabian Alb, Germany: Evidence for a high diversity of apes in the Late Miocene of Germany. Estud. Geol. 68, 113–147.

Pugh, K.D., 2022. Phylogenetic analysis of Middle-Late Miocene apes. J. Hum. Evol. 165, 103140.

Pugh, K.D., Catalano, S.A., Pérez de los Ríos, M., Fortuny, J., Shearer, B.M., Vecino Gazabón, A., Hammond, A.S., Moyà-Solà, S., Alba, D.M., Almécija, S., 2023. The reconstructed cranium of *Pierolapithecus* and the evolution of the great ape face. Proc. Natl. Acad. Sci. USA 120, e2218778120.

Sevim-Erol, A., Begun, D.R., Sönmez Sözer, Ç., Mayda, S., van den Hoek Ostende, L.W., Martin, R.M.G., Cihat Alçiçek, M., 2023. A new ape from Türkiye and the radiation of late Miocene hominines. Commun. Biol. 6, 842.

Urciuoli, A., Alba, D.M., 2023. Systematics of Miocene apes: State of the art of a neverending controversy. J. Hum. Evol. 175, 103309.

Zanolli, C., Bouchet, F., Fortuny, J., Bernardini, F., Tuniz, C., Alba, D.M., 2023. A reassessment of the distinctiveness of dryopithecine genera from the Iberian Miocene based on enamel-dentine junction geometric morphometric analyses. J. Hum. Evol. 177, 103326.

Figure captions

Figure 1. Dental remains of *Anoiapithecus brevirostris* from ACM/C4-Cp, including photographs (a–i) and three-dimensional model renders of the outer enamel surface (j, l, n, p) and enamel-dentine junction (k, m, o, q): a–e) IPS41713a, left C^1 in occlusal (a), labial (b), mesial (c), lingual (d), and distal (e) views; f, j, k) IPS41713c, left partial P^3 in occlusal view; g, l, m) IPS41713b, left P^4 crown in occlusal view; h, n, o) IPS41713d, left M^1 crown in occlusal view; i, p, q) IPS41713e, left M^2 lingual crown fragment in occlusal view. In occlusal views, mesial is on top. See Figure 2 and SOM Figure S6 for comparison with other Middle Miocene dryopithecine specimens from the same area. The 3D models can be accessed from MorphoSource (see SOM Table S2).

Figure 2. The male C^1 (a) and P^3–M^2 (g) of *Anoiapithecus brevirostris* described in this paper as compared with male C^1s (b–f) and upper cheek teeth (h–q) of Middle Miocene dryopithecines from Abocador de Can Mata: a) IPS41713a, *A. brevirostris* from ACM/C4-Cp; b) IPS43000, *A. brevirostris* (holotype) from ACM/C3-Aj (mirrored); c) IPS41714, *D. fontani* from ACM/C4-Ap; d) IPS35026, *Dryopithecus fontani* from ACM/C3-Ae (reversed); e–f) IPS21350, *Pierolapithecus catalaunicus* (holotype) from ACM/BCV1 (panel f is reversed); g) IPS41713b–e, P^3–M^2 of *A. brevirostris* from ACM/C4-Cp; h–i) IPS43000, P^3–M^2 of *A. brevirostris* (holotype) from ACM/C3-Aj (panel i is reversed); j–k) IPS35027, P^4–M^1 (j) and M^1–M^2 (k, reversed) of *A. brevirostris* from ACM/C1-E*; l) IPS41712, P^3–M^1 of *A. brevirostris* from ACM/C3-Aj; m) MGSB48486, M^2 of *D. fontani* from Can Mata s.l. (reversed); n–o) IPS35026, P^3–M^2 (n) and P^3–M^1 (o, reversed) of *D. fontani* from ACM/C3-Ae; p–q) IPS21350, P^3–M^2 of *P. catalaunicus* from ACM/BCV1 (panel k is reversed). All specimens are depicted as from the left side (indicated when mirrored). Canines are shown in occlusal (left top),

mesial (left bottom or middle), and labial (right) views, whereas cheek teeth are shown in occlusal view (mesial on top).

Figure 3. Results of the three-dimensional geometric morphometric analyses of M^1 enamel-dentine junction shape in *Anoiapithecus brevirostris* from ACM/C4-Cp as compared with other Middle Miocene dryopithecine specimens from the same area based on the (semi)landmark configuration after Procrustes alignment (see Materials and methods for further details). a) Canonical variate (CV) analysis based on extant great ape genera, with fossil specimens projected a posteriori, as depicted by a bivariate plot of CV2 vs. CV1. b) Principal component (PC) analysis based exclusively on the same fossil specimens, as depicted by a bivariate plot of PC2 vs. PC1. The maximum and minimum landmark configurations are depicted along each axis in occlusal and buccal views, while the percentage of variance accounted by each axis is reported within parentheses.

Table 1

Measurements[a] of left upper tooth series of *Anoiapithecus brevirostris* from ACM/C4-Cp.

Catalog no.	Tooth locus	MD	BL	BLm	BLd	BLI
IPS41713a	C^1	12.6	8.0	—	—	63.5
IPS41713c	P^3	>7.3	>9.9	—	—	—
IPS41713b	P^4	7.5	(11.0)	—	—	(146.7)
IPS41713d	M^1	10.3	(11.3)	(11.3)	>9.5	(109.7)
IPS41713e	M^2	>10.3	—	—	—	—

Abbreviations: MD = mesiodistal length (in mm); BL = buccolingual (or labiolingual) breadth (in mm), distinguishing between the mesial (BLm) and the distal (BLd) lobes in the case of molars; BLI = breadth/length index (in %), computed as maximum BL / MD × 100.

[a] Measurements between parentheses are estimates while those preceded by the 'greater than' symbol are lower than the original dimension due to incomplete preservation.

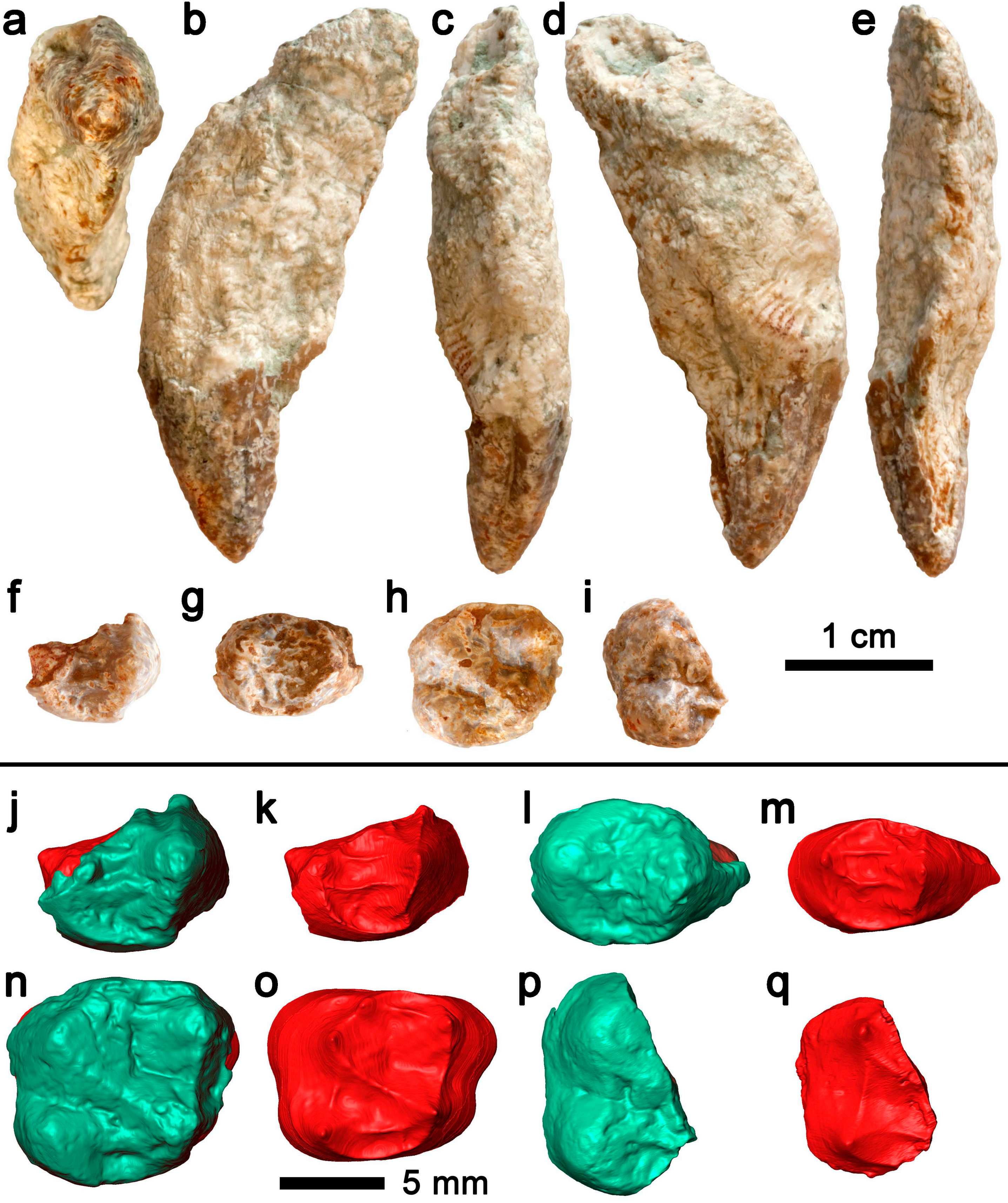
a
b
c
d
e
f
g
h
i
1 cm
j
k
l
m
n
o
p
q
5 mm

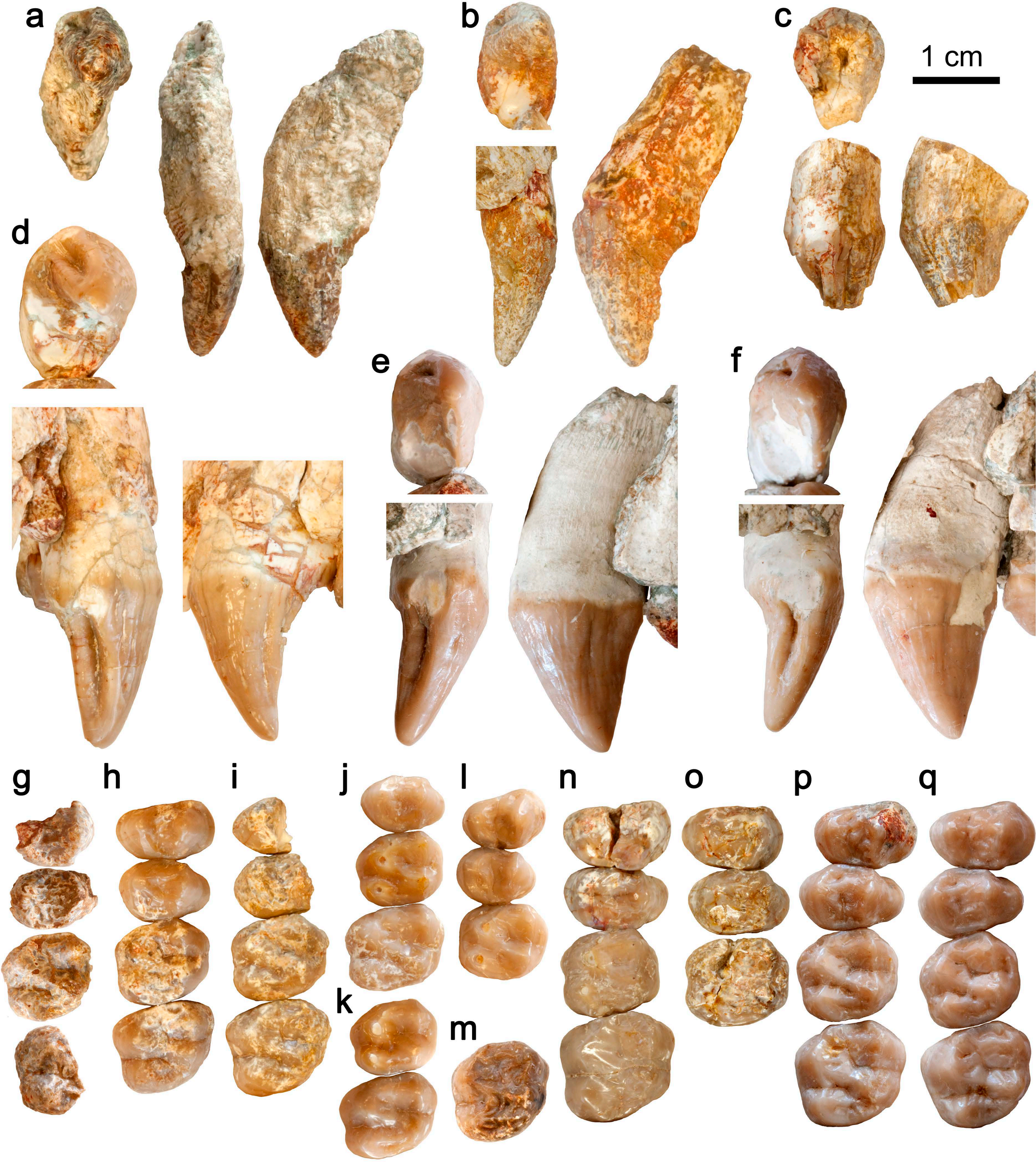
a
b
c
1 cm
d
e
f
g
h
i
j
l
n
o
p
q
k
m

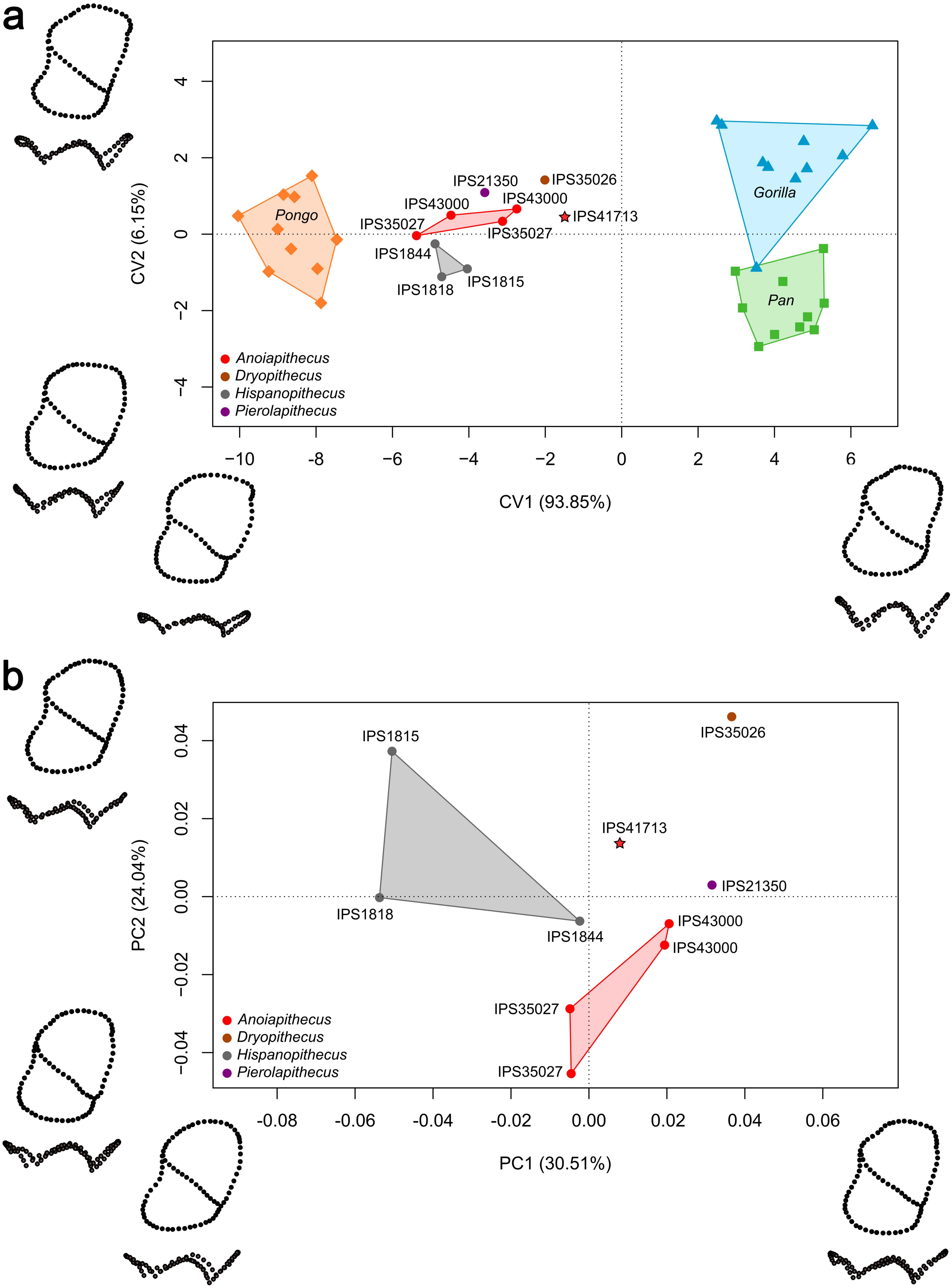
a
CV2 (6.15%)
CV1 (93.85%)
Pongo
Gorilla
Pan
IPS21350
IPS35026
IPS43000
IPS43000
IPS41713
IPS35027
IPS35027
IPS1844
IPS1815
IPS1818
Anoiapithecus
Dryopithecus
Hispanopithecus
Pierolapithecus
b
PC2 (24.04%)
PC1 (30.51%)
IPS1815
IPS35026
IPS41713
IPS21350
IPS1818
IPS1844
IPS43000
IPS43000
IPS35027
IPS35027
Anoiapithecus
Dryopithecus
Hispanopithecus
Pierolapithecus

Supplementary Online Material (SOM):

New remains of the Miocene great ape *Anoiapithecus brevirostris* from Abocador de Can Mata

David M. Alba [a,*], Florian Bouchet [a], Josep Fortuny [a], Josep M. Robles [a], Jordi Galindo [a], Àngel H. Luján [a], Salvador Moyà-Solà [a,b,c], Clément Zanolli [d,*]

[a] *Institut Català de Paleontologia Miquel Crusafont (ICP-CERCA), Universitat Autònoma de Barcelona, c/ Columnes s/n, 08193 Cerdanyola del Vallès, Barcelona, Spain*

[b] *Institució Catalana de Recerca i Estudis Avançats (ICREA), Pg. Lluís Companys 23, 08010 Barcelona, Spain*

[c] *Unitat d'Antropologia Biològica (Dept. BABVE), Universitat Autònoma de Barcelona, 08193 Cerdanyola del Vallès, Barcelona, Spain*

[d] *Univ. Bordeaux, CNRS, MCC, PACEA, UMR 5199, F-33600 Pessac, France*

***Corresponding authors**.

E-mail addresses: david.alba@icp.cat (D.M. Alba); clement.zanolli@gmail.com (C. Zanolli).

SOM S1

Preservation

The dental sample from ACM/C4-Cp includes five isolated specimens from the left side: an almost complete C^1 (IPS41713a), partial P^3 (IPS41713c) and M^2 (IPS41713e) crowns, and almost complete P^4 (IPS41713b) and M^1 (IPS41713d) crowns. No maxillary bone is preserved except for small, isolated fragments (IPS41713f), but the teeth were found in close spatial association and, in all probability, belong to a single individual. Based on canine size and shape, this individual can be sexed as male, probably corresponding to a young adult given the degree of wear of the upper molars and canine.

The teeth are poorly preserved due to taphonomic processes, as can be observed from the photograph of the C^1 taken in the field (SOM Fig. S2). This is probably attributable to acid corrosion during and/or soon after burial, as the fossil was recovered from a fresh claystone matrix not affected by recent edaphic processes. The C^1 preserves the crown and most of the root, except for its apical-most portion (Fig. 1a–e). However, the enamel surface is cracked and corroded, with chips of enamel missing, particularly close to the cervix. The root surface is even more affected by cracking and corrosion and, on its mesiolingual portion close to the cervix, it seemingly displays rodent gnawing marks. The roots of the cheek teeth (Figs. 1f–i and 2) are missing and the crowns display abundant acidic corrosion. The crowns of the P^4 and M^1 preserve most of the occlusal surface but are missing most of their basal-most portions toward the cervix, whereas those of the P^3 and M^2 are very incomplete. The P^3 preserves the paracone and the central and distal portions of the crown, but is missing the lingual and mesial walls as well as the basal-most portion of the buccal wall, while the M^2 consists of the buccal half of the crown.

SOM S2

Supplementary methods

2.1. Scanning and segmentation

The cheek teeth of IPS41713 were µCT-scanned at the Centro Nacional de Investigación sobre la Evolución Humana in Burgos (Spain) with a high-resolution X-ray µCT scanner model V|Tome|X s 240 (GE Sensing & Inspections Technologies). The µCT acquisition was carried out at 160 kV with a current of 120 µA, obtaining a voxel size of 18.50 µm. The X-ray beam was filtered by a 0.2 mm-thick copper absorber. Using the commercial software Avizo v. 7.1 (FEI Visualization Sciences Group, Hillsboro), a semiautomatic, threshold-based segmentation was carried out using a combination of the half-maximum height method (Spoor et al., 1993) and of the region of interest thresholding protocol (Fajardo et al., 2002; Coleman and Colbert, 2007).

2.2. Relative enamel thickness

Orientation and reconstruction Two-dimensional relative enamel thickness (2DRET) is a dimensionless variable devised to compare enamel thickness among species irrespective of size (Martin, 1985). In previous studies of 2DRET in Iberian dryopithecines (Alba et al., 2013, 2020; Fortuny et al., 2021), measurements were taken on a buccolingual virtual cross section passing through the tips of the mesial dentine horns and perpendicular to the best-fit plane of the cervical line (Benazzi et al., 2014). However, given that the cervix is not completely preserved in IPS41713d, we relied instead on the developmental plane (defined by placing a landmark on the apex of each trigon cusps) to generate a buccolingual cross section perpendicular to it. Results obtained with either the developmental plane or the cervical plane were previously shown to be comparable (Smith et al., 2012). Furthermore, it was necessary to reconstruct the basal portion of the dentine and enamel cap, as well as the enamel at the apex of the protocone, to account for light wear as in previous studies (e.g., Fortuny et al., 2021). Following previously established protocols (e.g., Smith et al., 2012), enamel was reconstructed following the natural curve of the crown and only minimal reconstructions were made. Two independent reconstructions were made by two authors of the paper (F.B. and C.Z.) and the average value was then taken.

Computation of relative enamel thickness Two-dimensional relative enamel thickness was computed following Martin's (1985) protocol on a virtual buccolingual section passing through the mesial dentine horns, reconstructed as described above. The following formulas was used (Martin, 1985; Smith et al., 2005; Fortuny et al., 2021): 2DRET = 2DAET × $100/b^{1/2}$ and 2DAET = c/e, where 2DAET = bidimensional average enamel thickness (in mm), b = dentine and pulp area (in mm^2), c = enamel cap area (in mm^2), and e = enamel-dentine junction length (in mm).

2.3. Shape analysis

(Semi)landmark protocol The three-dimensional geometric morphometric analysis of enamel-dentine junction (EDJ) virtual surfaces was performed using a protocol based on four landmarks placed at the apices of the main cusp dentine horns plus 75 semilandmarks placed along occlusal crests and the mesial and distal marginal ridges (SOM Fig. S3): 10 on the prehypocrista, 10 on the postparacrista + premetacrista, 20 on the preprotocrista + mesial marginal ridge + preparacrista, 20 on the postmetacrista + distal marginal ridge + posthypocrista, and 15 on the crista obliqua. Landmark data were imported into R v. 4.1.1 (R Core Team, 2021) to perform Procrustes alignments using the 'ProcSym' function of the R package 'Morpho' v. 2.9 (Schlager, 2021).

Comparative sample The comparative sample of Iberian dryopithecines for the morphometric analysis consists of nine M^1s for which the EDJ was previously analyzed (Fortuny et al., 2021; Zanolli et al., 2023; see SOM Table S3): the right and left antimeres of two individuals of *Anoiapithecus brevirostris* (IPS43000 [holotype] and IPS35027); a single specimen of *Pierolapithecus catalaunicus* (IPS21350 [holotype]) and another of *Dryopithecus fontani* (IPS35026); and three specimens of *Hispanopithecus*, including two of *Hispanopithecus crusafonti* (IPS1815 and IPS1818) and another of *Hispanopithecus laietanus* (IPS1844). In turn, the extant hominid comparative sample consists of 10 M^1s for each of the three living great ape genera *Pan*, *Gorilla*, and *Pongo* (i.e., 30 M^1s in total; for details of the extant comparative sample composition, see Zanolli et al., 2023: SOM Table S2).

<u>Multivariate analyses</u> The multivariate analyses were performed on landmark data taken from the EDJ surface after Procrustes alignment. A canonical variate analysis (CVA) was performed from a prior principal component analysis (PCA), with three groups (corresponding to the three extant genera) defined a priori and the fossils projected a posteriori. Another PCA based exclusively on the fossil specimens was also performed. The CVA allows to ascertain the portion of the morphospace occupied by dryopithecines relative to extant taxa but has the problem that the fossils do not participate in the definition of the morphospace and that the latter is distorted to maximize the distinction among extant genera but not extinct ones. In contrast, the PCA defines the morphospace exclusively on the basis of fossil specimens and is thus arguably more suitable to ascertain the closest similarities of the newly described specimen to dryopithecine genera. Given that CVA requires a smaller number of variables than specimens, it was based on a subset of the first principal component (PC) scores that maximized correct classification (e.g., Zanolli et al., 2023). The first seven PCs (accounting for 93% of variance) were selected to run the CVA (see the first two PCs in SOM Fig. S10), whose accuracy was ascertained based on the percentage of correctly classified extant cases (both without and with cross validation). For fossil specimens, typicality probabilities were reported to ascertain if they fit with the variation of the extant

great ape genera separately. The PCAs and CVA were computed using the R packages ‘ade4’ v. 1.7-18 (Dray and Dufour, 2007) and ‘Morpho’, respectively.

SOM S3

Supplementary results of the shape analyses

3.1. Canonical variate analysis

The CVA based on M^1 EDJ shape of extant great ape genera correctly classifies 96.7% of the original cases (93.3% after cross-validation; SOM Table S5). Dryopithecines display an intermediate position between orangutans and African apes along the first canonical variate (CV1; Fig. 3a; SOM Table S6). This axis, which explains most of the variance (94%), discriminates between orangutans (very negative scores) and African apes (positive scores), with dryopithecines displaying moderately negative scores. It is mainly driven by dentine horn height (and hence occlusal relief) and other occlusal details, with orangutans displaying toward negative scores lower dentine horns and shallower relief, as well as a relatively broader trigon basin with slightly more peripheral paracone and protocone horns and a more prominent protoconule, and a relatively narrower distal fovea with less peripheral metacone and hypocone horns (Fig. 3a).

In turn, CV2 (6% of variance) only discriminates between chimpanzees (negative scores) and gorillas (generally positive scores), with only minimal overlap with one another but extensive overlap with orangutans at intermediate scores (Fig. 3; SOM Table S6). This axis is driven by the relative width of the occlusal basins, with gorillas displaying relatively narrower foveae with a slightly less peripheral metacone toward positive scores. Along this axis, dryopithecines are intermediate between chimpanzees and gorillas (i.e., they display moderately positive or negative scores), completely overlapping with orangutans and to some extent with either gorillas or chimpanzees. Overall, dryopithecines occupy their own portion of the morphospace—distinct from any extant great ape genus but to a large extent intermediate among them—with extinct genera overlapping along CV1 but not CV2.

Typicality probabilities clearly show that none of the dryopithecine specimens, including IPS41713d, fits well with the variation of any extant taxon (SOM Table S7).

3.2. Principal component analysis

This analysis (Fig. 3b) denotes some differences between Middle and Late Miocene dryopithecines along the first principal component (PC1), which accounts for 31% of variance and is driven by multiple occlusal details, including the arrangement of the main cusps (more peripheral and mesial paracone, more median protocone, and more distal hypocone), the less marked protoconule, and the narrower distal fovea toward negative scores. Along this component, *Hispanopithecus* shows negative PC1 scores while the Middle Miocene specimens display positive or minimally negative scores, with only slight overlap between some specimens of *Anoiapithecus* and the single *H. laietanus* specimen. In turn, PC2 embeds 24% of variance and is driven by different occlusal details than PC1, including the higher paracone, the lower protocone, the more distal metacone with a more oblique crista obliqua, and the relatively shorter distal fovea toward positive scores. This axis separates *Anoiapithecus* (negative scores) from other M^1s, although almost overlapping with the single specimen of *H. laietanus*. The single M^1 of *Dryopithecus* most clearly differs from the rest of the sample by displaying the highest PC1 and PC2 scores, while IPS41713d displays moderately positive PC1 and PC2 scores—the former only overlapping with *Anoiapithecus* and the latter with *Hispanopithecus*. The next two components (PC3 and PC4) explain respectively 15% and 14% of variance but do not clearly discriminate among taxa. All the PC scores are reported in SOM Table S8.

SOM Figure S1. Photograph of the construction of the Can Mata landfill and associated paleontological fieldwork in February 2006, showing the location of localities ACM/C4-Cp and C4-Ap. Photograph © Institut Català de Paleontologia Miquel Crusafont.

SOM Figure S2. Photograph of the male C[1] IPS41713a as found at the field before being prepared. Photograph © Institut Català de Paleontologia Miquel Crusafont.

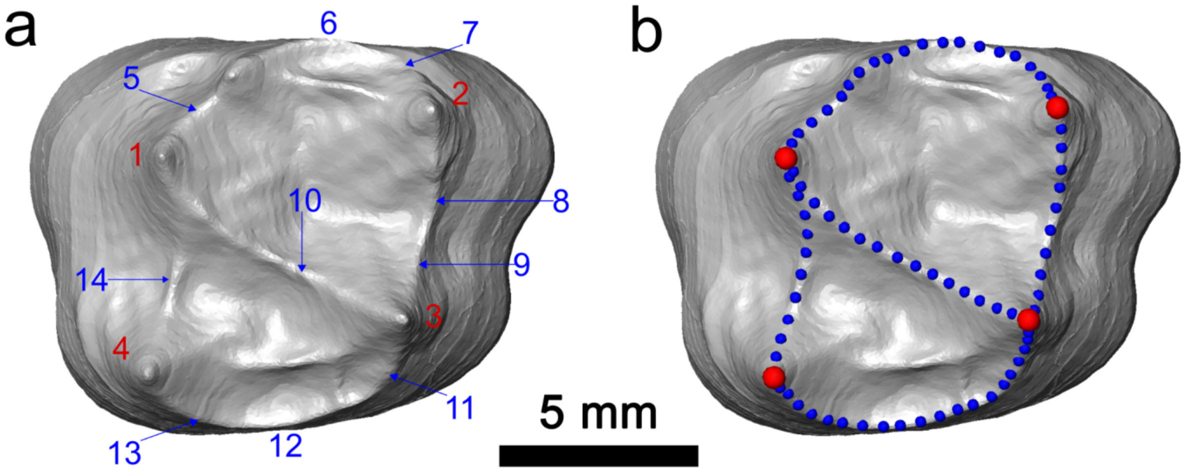

SOM Figure S3. Landmark protocol used for the analysis of M^1 enamel-dentine junction (EDJ) shape in dryopithecines from the Vallès-Penedès Basin, as exemplified by a rendering in occlusal view of the EDJ surface in IPS41713 from ACM/C4-Cp. a) EDJ dentine horns (red numbers) and crests/ridges (blue numbers) used for landmarking. b) Placement of landmarks (red dots) and semilandmarks (blue dots). 1 = protocone; 2 = paracone; 3 = metacone; 4 = hypocone; 5 = preprotocrista; 6 = mesial marginal ridge; 7 = preparacrista; 8 = postparacrista; 9 = premetacrista; 10 = crista obliqua; 11 = postmetacrista; 12 =distal marginal ridge; 13 = posthypocrista; 14 = prehypocrista.

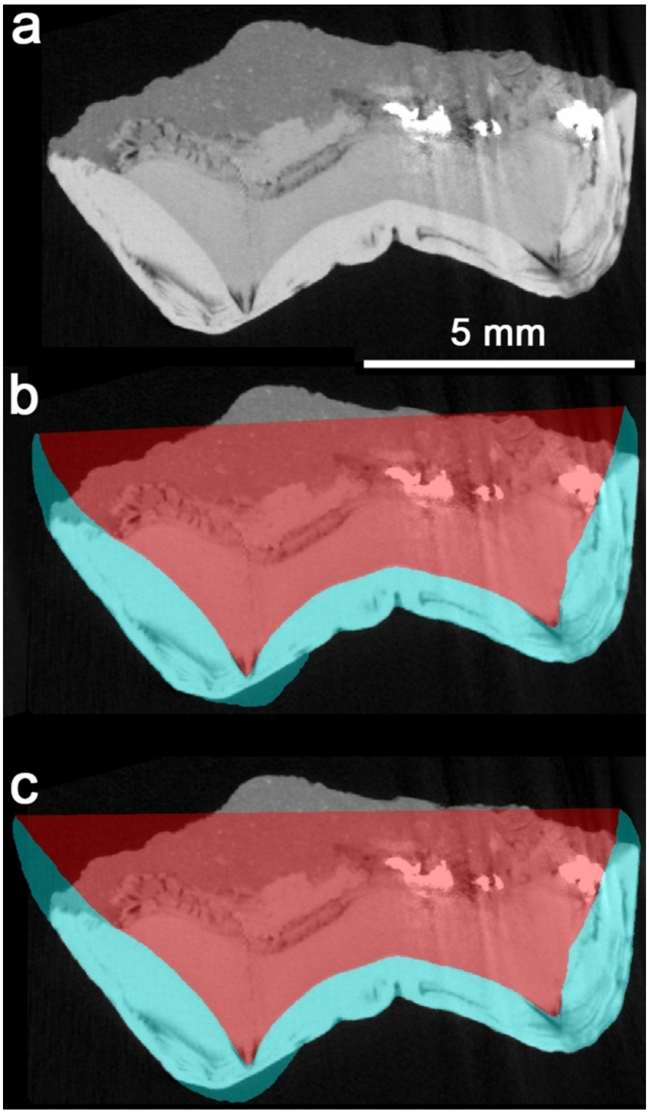

SOM Figure S4. The µCT buccolingual section of the left M^1 of *Anoiapithecus brevirostris* from ACM/C4-Cp (IPS41713d) used to compute relative enamel thickness, in mesial view (i.e., lingual is on the left): a) virtual section passing through the dentine horn apices of the mesial cusps and perpendicular to the developmental plane; b–c) reconstruction of the enamel (cyan) and dentine (red) in semitransparency and overlapping the aforementioned section, independently performed by C.Z. (b) and F.B. (c).

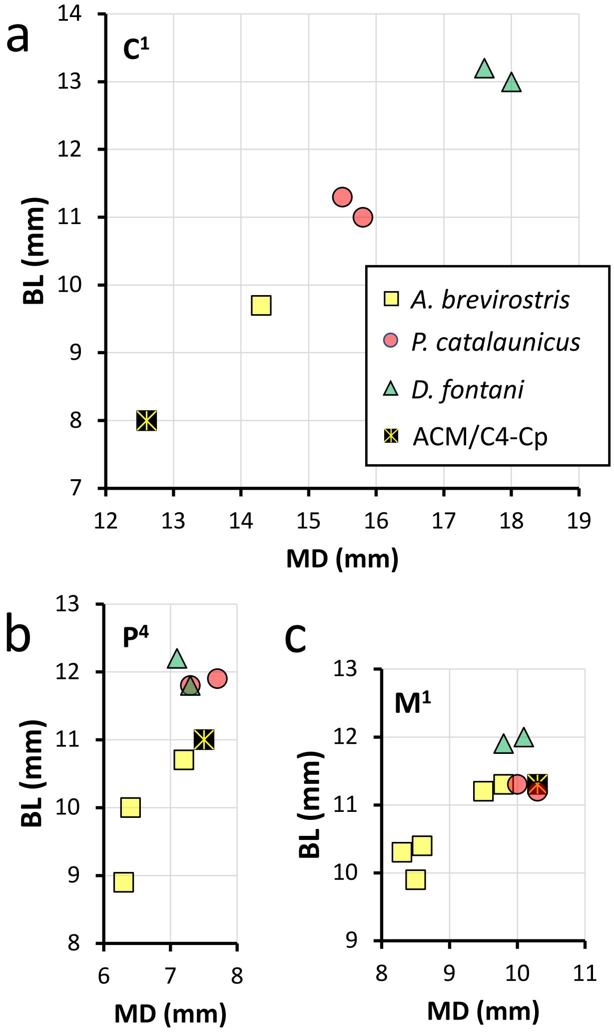

SOM Figure S5. Bivariate plots of buccolingual breadth (BL) vs. mesiodistal length (MD) in the male C^1 (a), the P^4 (b), and the M^1 c) of *Anoiapithecus brevirostris* from ACM/C4-Cp as compared with other Middle Miocene dryopithecines from the Vallès-Penedès Basin. See SOM Table S1 for measurements.

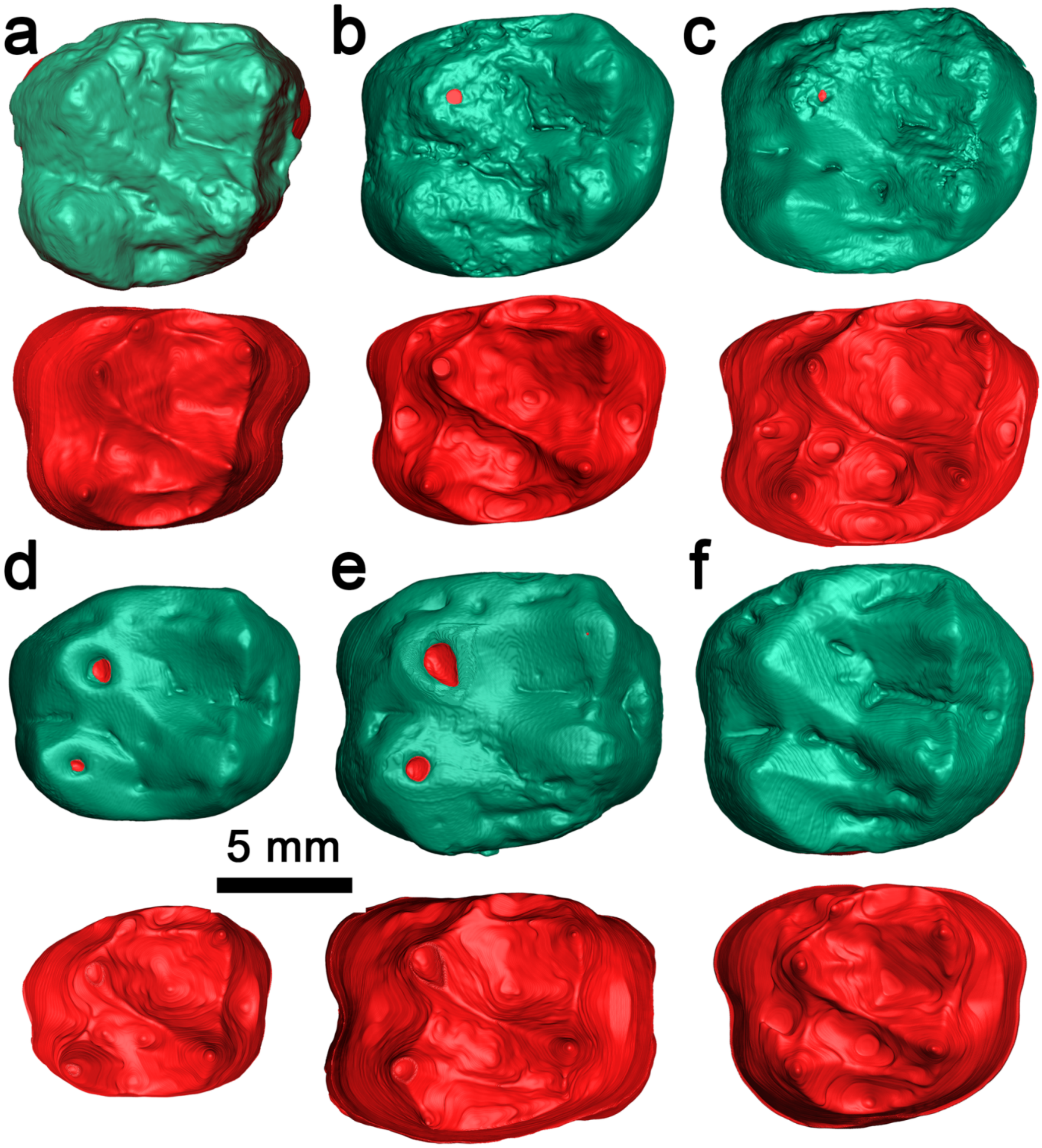

SOM Figure S6. Outer enamel surface (OES, in green) and enamel-dentine junction (EDJ, in red) three-dimensional surface renders of the M^1 of *Anoiapithecus brevirostris* described in this paper as compared with homologous teeth of Middle Miocene dryopithecines from the same area (reproduced from Fortuny et al., 2021: Fig. 4 and Supplementary Fig. 9): a) IPS41713d, left M^1 of *A. brevirostris* from ACM/C4-Cp; b–c) IPS43000 (holotype), left (b) and right (c, reversed) M^1 of *A. brevirostris* from ACM/C3-Aj; d) IPS35027, left M^1 of *A. brevirostris* from ACM/C1-E*; e) IPS35026, left M^1 of *Dryopithecus fontani* from ACM/C3-

Ae; f) IPS21350 (holotype), left M^1 of *Pierolapithecus catalaunicus* from ACM/BCV1. All specimens are depicted as from the left side (indicated when mirrored) in occlusal view (mesial on top).

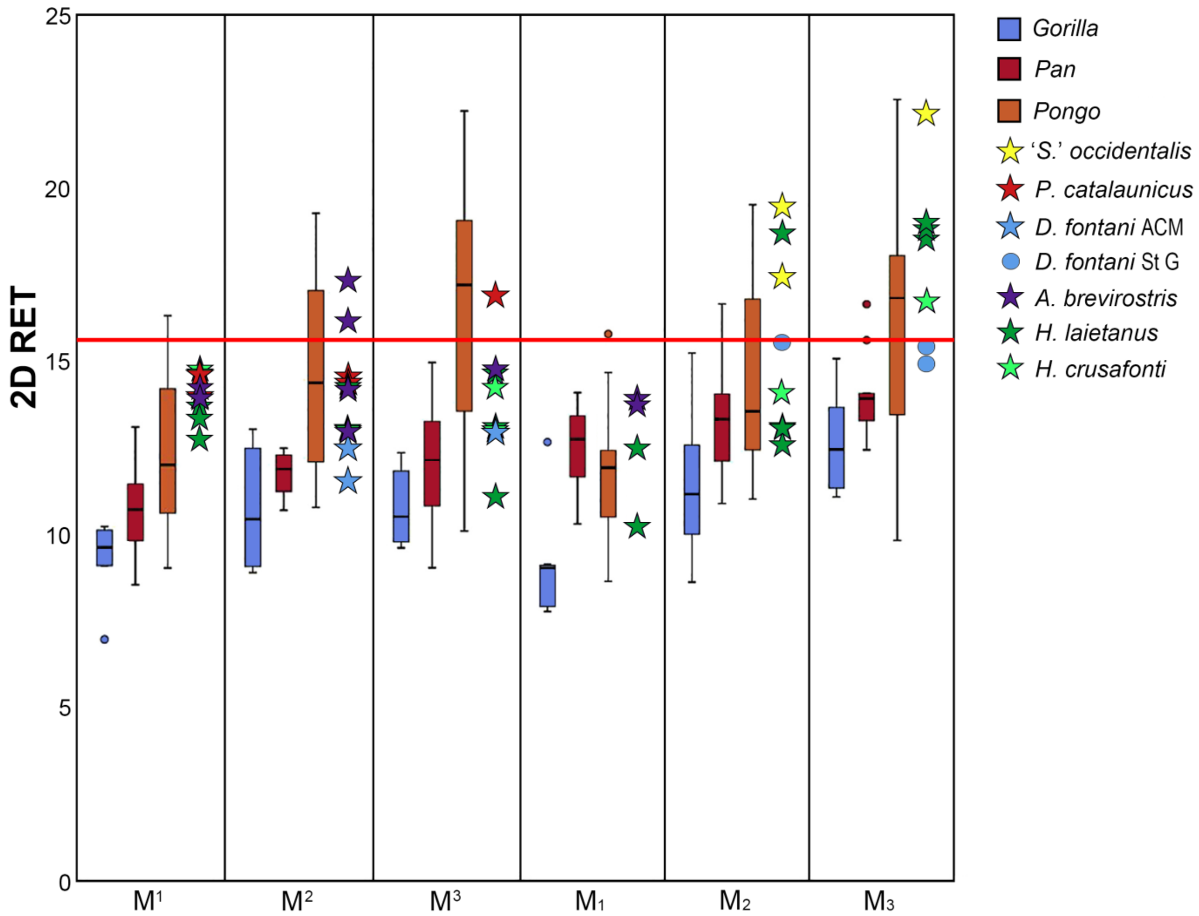

SOM Figure S7. Box-and-whisker plots of molar two-dimensional relative enamel thickness (2DRET) in the M^1 (IPS41713d) of *Anoiapithecus brevirostris* from ACM/C4-Cp (red horizontal line) as compared with dryopithecines from Spain and southern France as well as extant great apes. Boxes represent the interquartile range (IQR), centerline is the median, whiskers denote the maximum and minimum values within 1.5 times the IQR, and dots are outliers. Abbreviations: ACM = Abocador de Can Mata; St G = Saint-Gaudens.

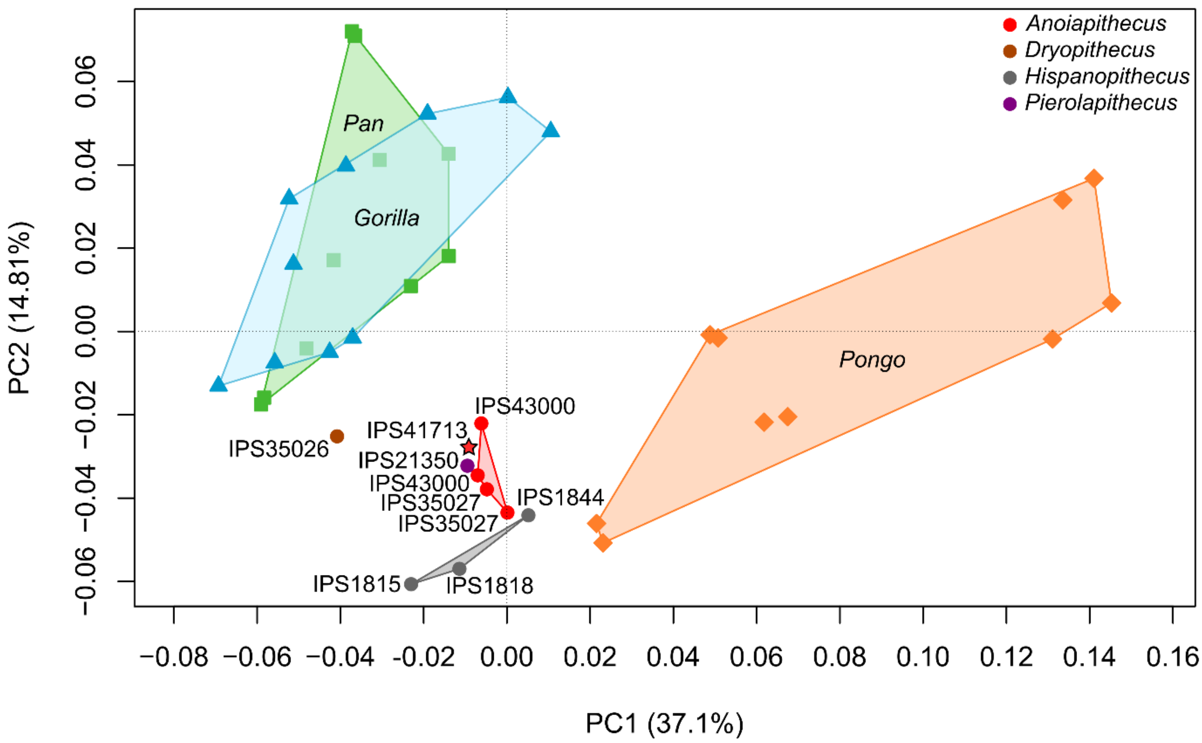

SOM Figure S8. Principal component (PC) analysis of M^1 enamel-dentine junction shape in extant great ape genera based on the (semi)landmark configuration after Procrustes alignment, with fossil specimens projected a posteriori. Only the first two axes (PC2 vs. PC1, with the percentage of variance accounted by each axis reported within parentheses) are shown. However, the first seven PCs (accounting for 93% of variance) were selected to run the canonical variate analysis depicted in Figure 3a.

SOM Table S1

Measurements[a] of left upper tooth series IPS41713 from Abocador de Can Mata locality ACM/C4-Cp as compared with those of the same tooth loci of other dryopithecine specimens from the same area.

Species	Locality	Catalog no.	Tooth locus	Side	MD	BL	BLI	Source[b]
Anoiapithecus brevirostris	ACM/C4-Cp	IPS41713a	C^1	L	12.6	8.0	63.5	This study
Anoiapithecus brevirostris	ACM/C3-Aj	IPS43000	C^1	R	14.3	9.7	67.8	Moyà-Solà et al. (2009a)
Pierolapithecus catalaunicus	ACM/BCV1	IPS21350	C^1	R	15.5	11.3	72.9	Moyà-Solà et al. (2004)
Pierolapithecus catalaunicus	ACM/BCV1	IPS21350	C^1	L	15.8	11.0	69.6	Moyà-Solà et al. (2004)
Dryopithecus fontani	ACM/C3-Ae	IPS35026	C^1	R	18.0	13.0	72.2	Moyà-Solà et al. (2009b)
Dryopithecus fontani	ACM/C3-Ae	IPS35026	C^1	L	17.6	13.2	75.0	Moyà-Solà et al. (2009b)
Dryopithecus fontani	ACM/C4-Ap	IPS41714	C^1	L	>13.8	12.4	—	Alba and Moyà-Solà (2012)[c]
Anoiapithecus brevirostris	ACM/C4-Cp	IPS41713c	P^3	L	>7.3	>9.9	—	This study
Anoiapithecus brevirostris	ACM/C3-Aj	IPS43000	P^3	L	7.0	11.7	167.1	Moyà-Solà et al. (2009a)
Anoiapithecus brevirostris	ACM/C3-Aj	IPS41712	P^3	L	6.4	9.4	146.9	Alba et al. (2013)
Pierolapithecus catalaunicus	ACM/BCV1	IPS21350	P^3	R	7.9	11.9	150.6	Moyà-Solà et al. (2004)
Pierolapithecus catalaunicus	ACM/BCV1	IPS21350	P^3	L	7.4	11.5	155.4	Moyà-Solà et al. (2004)
Dryopithecus fontani	ACM/C3-Ae	IPS35026	P^3	R	7.5	12.0	160.0	Moyà-Solà et al. (2009b)

Dryopithecus fontani	ACM/C3-Ae	IPS35026	P^3	L	8.0	12.0	152.5	Moyà-Solà et al. (2009b)
Anoiapithecus brevirostris	ACM/C4-Cp	IPS41713b	P^4	L	7.5	(11.0)	(146.7)	This study
Anoiapithecus brevirostris	ACM/C3-Aj	IPS43000	P^4	R	7.3	>9.2	—	Moyà-Solà et al. (2009a)
Anoiapithecus brevirostris	ACM/C3-Aj	IPS43000	P^4	L	7.2	10.7	148.6	Moyà-Solà et al. (2009a)
Anoiapithecus brevirostris	ACM/C3-Aj	IPS41712	P^4	L	6.3	8.9	141.3	Alba et al. (2013)
Anoiapithecus brevirostris	ACM/C1-E*	IPS35027	P^4	L	6.4	10.0	156.3	Alba et al. (2013)
Pierolapithecus catalaunicus	ACM/BCV1	IPS21350	P^4	R	7.7	11.9	154.5	Moyà-Solà et al. (2004)
Pierolapithecus catalaunicus	ACM/BCV1	IPS21350	P^4	L	7.3	11.8	161.6	Moyà-Solà et al. (2004)
Dryopithecus fontani	ACM/C3-Ae	IPS35026	P^4	R	7.3	11.8	161.6	Moyà-Solà et al. (2009b)
Dryopithecus fontani	ACM/C3-Ae	IPS35026	P^4	L	7.1	12.2	171.8	Moyà-Solà et al. (2009b)
Anoiapithecus brevirostris	ACM/C4-Cp	IPS41713d	M^1	L	10.3	(11.3)	(109.7)	This study
Anoiapithecus brevirostris	ACM/C3-Aj	IPS43000	M^1	R	9.5	11.2	117.9	Moyà-Solà et al. (2009a)
Anoiapithecus brevirostris	ACM/C3-Aj	IPS43000	M^1	L	9.8	11.3	115.3	Moyà-Solà et al. (2009a)
Anoiapithecus brevirostris	ACM/C3-Aj	IPS41712	M^1	L	8.5	9.9	116.5	Alba et al. (2013)
Anoiapithecus brevirostris	ACM/C1-E*	IPS35027	M^1	R	8.6	10.4	120.9	Alba et al. (2013)
Anoiapithecus brevirostris	ACM/C1-E*	IPS35027	M^1	L	8.3	10.3	124.1	Alba et al. (2013)
Pierolapithecus catalaunicus	ACM/BCV1	IPS21350	M^1	R	10.3	11.2	108.7	Moyà-Solà et al. (2004)

Pierolapithecus catalaunicus	ACM/BCV1	IPS21350	M^1	L	10.0	11.3	113.0	Moyà-Solà et al. (2004)
Dryopithecus fontani	ACM/C3-Ae	IPS35026	M^1	R	10.1	12.0	118.8	Moyà-Solà et al. (2009b)
Dryopithecus fontani	ACM/C3-Ae	IPS35026	M^1	L	9.8	11.9	119.0	Moyà-Solà et al. (2009b)
Anoiapithecus brevirostris	ACM/C4-Cp	IPS41713e	M^2	L	>10.3	—	—	This study
Anoiapithecus brevirostris	ACM/C3-Aj	IPS43000	M^2	R	11.3	12.2	109.0	Moyà-Solà et al. (2009a)
Anoiapithecus brevirostris	ACM/C3-Aj	IPS43000	M^2	L	10.9	12.2	111.9	Moyà-Solà et al. (2009a)
Anoiapithecus brevirostris	ACM/C1-E*	IPS35027	M^2	R	9.3	11.7	125.8	Alba et al. (2013)
Anoiapithecus brevirostris	ACM/C1-E*	IPS35027	M^2	L	9.5	11.6	122.1	Alba et al. (2013)
Pierolapithecus catalaunicus	ACM/BCV1	IPS21350	M^2	R	11.3	12.4	109.7	Moyà-Solà et al. (2004)
Pierolapithecus catalaunicus	ACM/BCV1	IPS21350	M^2	L	11.3	12.5	110.6	Moyà-Solà et al. (2004)
Dryopithecus fontani	ACM/C3-Ae	IPS35026	M^2	L	12.7	13.8	108.7	Moyà-Solà et al. (2009b)
Dryopithecus fontani	Can Mata s.l.	MGSB48486	M^2	R	11.4	11.6	101.8	Van der Made and Ribot, 1999

Abbreviations: R = right; L = left; MD = mesiodistal length (in mm); BL = maximum buccolingual (or labiolingual) breadth (in mm); BLI = breadth/length index (in %), computed as BL / MD × 100; ACM = Abocador de Can Mata; BCV1 = Barranc de Can Vila 1; C1 = Cell 1; C3 = Cell 3; C4 = Cell 4.

[a] Measurements between parentheses are estimates while those preceded by the 'greater than' symbols are lower than the original dimension due to incomplete preservation.

[b] All the measurements were taken or confirmed by D.M.A. to ensure consistency, as in some cases there are small discrepancies with those provided in the original descriptions cited in the last column.

[c] This specimen was figured and cursorily described by Alba and Moyà-Solà (2012) in response to Pickford (2012), but no measurements were provided by the former.

SOM Table S2

Digital object identifiers (DOIs) of the three-dimensional models of the outer enamel surface (OES) and enamel-dentine junction (EDJ) of the cheek teeth of *Anoiapithecus brevirostris* from ACM/C4-Cp.

Catalog no.	Tooth locus	Type of model	DOI
IPS41713c	P^3	OES	https://doi.org/10.17602/M2/M575286
IPS41713c	P^3	EDJ	https://doi.org/10.17602/M2/M575289
IPS41713b	P^4	OES	https://doi.org/10.17602/M2/M575272
IPS41713b	P^4	EDJ	https://doi.org/10.17602/M2/M575283
IPS41713d	M^1	OES	https://doi.org/10.17602/M2/M575292
IPS41713d	M^1	EDJ	https://doi.org/10.17602/M2/M575295
IPS41713e	M^2	OES	https://doi.org/10.17602/M2/M575299
IPS41713e	M^2	EDJ	https://doi.org/10.17602/M2/M575302

SOM Table S3

Comparative sample of Miocene dryopithecine M^1s from the Vallès-Penedès Basin used in the shape analysis of enamel-dentine junction (available from MorphoSource after Fortuny et al., 2021).

Species	Catalog no.	Side	Site	Age	DOI
A. brevirostris	IPS43000	R	ACM/C3-Aj	12.0 Ma	https://doi.org/10.17602/M2/M166408
A. brevirostris	IPS43000	L	ACM/C3-Aj	12.0 Ma	https://doi.org/10.17602/M2/M166414
A. brevirostris	IPS35027	R	ACM/C1-E*	12.4–12.3 Ma	https://doi.org/10.17602/M2/M166403
A. brevirostris	IPS35027	L	ACM/C1-E*	12.4–12.3 Ma	https://doi.org/10.17602/M2/M166405
D. fontani	IPS35026	L	ACM/C3-Ae	11.9 Ma	https://doi.org/10.17602/M2/M166397
P. catalaunicus	IPS21350	L	ACM/BCV1	12.0 Ma	https://doi.org/10.17602/M2/M166321
H. crusafonti	IPS1815	L	CP1	10.4–10.0 Ma	https://doi.org/10.17602/M2/M166372
H. crusafonti	IPS1818	L	CP1	10.4–10.0 Ma	https://doi.org/10.17602/M2/M166229
H. laietanus	IPS1844	R	CLL1	9.8 Ma	https://doi.org/10.17602/M2/M166318

Abbreviations: DOI = digital object identifier; R = right; L = left; ACM = Abocador de Can Mata macrosite; BCV1 = Barranc de Can Vila 1; C1 = Cell 1; C3 = Cell 3; CLL1 = Can Llobateres 1; CP1 = Can Poncic 1.

SOM Table S4

Measurements taken on the reconstructed M^1 of *Anoiapithecus brevirostris* from ACM/C4-Cp (IPS41713d) to compute enamel thickness.[a]

	Reconstruction 1	Reconstruction 2	Average
Enamel area (c, in mm^2)	14.65	14.90	14.78
Dentine and pulp area (b, in mm^2)	30.74	30.43	30.59
Enamel-dentine junction length (e, in mm)	17.20	17.19	17.20
Average enamel thickness (in mm): 2DAET = c / e	0.85	0.87	0.86
Relative enamel thickness (2DRET = 2DAET × $100/b^{1/2}$)	15.36	15.72	15.54

[a] Measurements were taken from two reconstructions, which were independently performed by C.Z. (reconstruction 1) and F.B. (reconstruction 2; see the virtual sections used in SOM Fig. S4), yielding very similar results. The average values were then used to compute 2DRET.

SOM Table S5

Classification results of the canonical variate analysis of M^1 enamel-dentine junction shape in extant great ape genera (n = 30).[a]

Without cross validation	*Gorilla*	*Pan*	*Pongo*	Total correct
Gorilla	9 (90.0%)	1 (10.0%)	0 (0.0%)	9 (90.0%)
Pan	0 (0%)	10 (100%)	0 (0.0%)	10 (100%)
Pongo	0 (0%)	0 (0%)	10 (100%)	10 (100%)
Total	9 (30.0%)	11 (36.7%)	10 (33.3%)	**29 (96.7%)**
With cross validation	*Gorilla*	*Pan*	*Pongo*	Total correct
Gorilla	9 (90.0%)	1 (10.0%)	0 (0%)	9 (90.0%)
Pan	1 (10.0%)	9 (90.0%)	0 (0%)	9 (90%)
Pongo	0 (0%)	0 (0%)	10 (100%)	10 (100%)
Total	10 (33.3%)	10 (33.3%)	10 (33.3%)	**28 (93.3%)**

[a] Percentage classification results are given within parentheses.

[b] The total of correctly classified cases is bolded.

SOM Table S6

Canonical variate (CV) scores for IPS41713d from ACM/C4-Cp, other dryopithecines from the Vallès-Penedès Basin, and the centroids of the three groups defined a priori (extant great ape genera) resulting from a canonical variate analysis of M^1 enamel-dentine junction shape. The percentage of variance explained by each CV is reported within parentheses.

Species	Catalog no.	CV1 (93.85%)	CV2 (6.15%)
A. brevirostris	IPS41713	-1.490195	0.463888
A. brevirostris	IPS35027	-5.370976	-0.038744
A. brevirostris	IPS35027	-3.118701	0.335988
A. brevirostris	IPS43000	-2.745946	0.660717
A. brevirostris	IPS43000	-4.467845	0.495539
P. catalaunicus	IPS21350	-3.583646	1.088764
D. fontani	IPS35026	-2.010734	1.417876
H. crusafonti	IPS1815	-4.040992	-0.907053
H. crusafonti	IPS1818	-4.710648	-1.114975
H. laietanus	IPS1844	-4.885182	-0.253428
Gorilla centroid	—	4.266756	1.904310
Pan centroid	—	4.309286	-1.898025
Pongo centroid	—	-8.576042	-0.006286

SOM Table S7

Classification results for IPS41713d from ACM/C4-Cp and other Middle Miocene dryopithecines from the Vallès-Penedès Basin based on a canonical variate analysis of M^1 enamel-dentine junction shape in extant great ape genera, including typicality probabilities[a] and the Mahalanobis squared distances to extant group centroids.

Catalog no.	Species	Typicality probabilities		
		Gorilla	*Pan*	*Pongo*
IPS41713	*A. brevirostris*	<0.01	<0.01	<0.01
IPS35027 (left)	*A. brevirostris*	<0.01	<0.01	0.03
IPS35027 (right)	*A. brevirostris*	<0.01	<0.01	<0.01
IPS43000 (left)	*A. brevirostris*	<0.01	<0.01	<0.01
IPS43000 (right)	*A. brevirostris*	<0.01	<0.01	<0.01
IPS35026	*D. fontani*	<0.01	<0.01	<0.01
IPS1815	*H. crusafonti*	<0.01	<0.01	<0.01
IPS1818	*H. crusafonti*	<0.01	<0.01	<0.01
IPS1844	*H. laietanus*	<0.01	<0.01	0.01
IPS21350	*P. catalaunicus*	<0.01	<0.01	<0.01
Catalog no.	**Species**	**Distances**		
		Gorilla	*Pan*	*Pongo*
IPS41713	*A. brevirostris*	5.93	6.26	7.10
IPS35027 (left)	*A. brevirostris*	9.83	9.85	3.21
IPS35027 (right)	*A. brevirostris*	7.55	7.75	5.47
IPS43000 (left)	*A. brevirostris*	7.12	7.50	5.87
IPS43000 (right)	*A. brevirostris*	8.85	9.10	4.14
IPS35026	*D. fontani*	6.30	7.13	6.72

IPS1815	*H. crusafonti*	8.77	8.41	4.62
IPS1818	*H. crusafonti*	9.47	9.05	4.02
IPS1844	*H. laietanus*	9.40	9.34	3.70
IPS21350	*P. catalaunicus*	7.89	8.44	5.11

Abbreviations: R = right; L = left.

[a] Typicality probabilities, which add to unity, denote the probability of having the given score assuming the specimen belongs to a particular group, and hence indicate if a fossil specimen fits well with the variation of each extant group (rejected when $p < 0.05$).

SOM Table S8

Principal component (PC) scores for IPS41713d from ACM/C4-Cp and other dryopithecines from the Vallès-Penedès Basin, resulting from a principal component analysis of M^1 enamel-dentine junction shape. The percentage of variance explained by each PC is reported within parentheses.

Species	Catalog no.	PC1 (30.5%)	PC2 (24.0%)	PC3 (15.4%)	PC4 (13.6%)	PC5 (6.0%)	PC6 (4.4%)	PC7 (3.1%)	PC8 (1.9%)	PC9 (1.1%)
A. brevirostris	IPS41713	0.0078740	0.0136901	0.0193508	-0.0337240	-0.0143747	0.0059635	0.0046638	-0.0118356	0.0038692
A. brevirostris	IPS35027	-0.0045621	-0.0454002	0.0270590	0.0158740	0.0102334	-0.0060722	-0.0076233	-0.0094472	-0.0035005
A. brevirostris	IPS35027	-0.0048789	-0.0287682	0.0166910	0.0114523	-0.0021312	0.0068738	0.0162866	0.0102727	0.0065877
A. brevirostris	IPS43000	0.0194095	-0.0124312	-0.0199514	0.0061576	-0.0166729	0.0131280	0.0025595	0.0010361	-0.0115351
A. brevirostris	IPS43000	0.0205686	-0.0069459	-0.0152722	0.0071349	-0.0108491	0.0025095	-0.0196284	0.0036523	0.0087131
P. catalaunicus	IPS21350	0.0315652	0.0029753	0.0018880	-0.0188488	-0.0012008	-0.0263331	0.0022653	0.0074333	-0.0031079
D. fontani	IPS35026	0.0366237	0.0461426	-0,0001280	0.0315652	0.0127305	0.0011791	0.0054048	-0.0048270	0.0011856
H. crusafonti	IPS1815	-0.0505218	0.0372798	0.0257830	0.0015282	-0.0023431	0.0030270	-0.0083608	0.0075355	-0.0040949
H. crusafonti	IPS1818	-0.0537303	-0.0002556	-0.0364222	0.0079002	-0.0040345	-0.0115364	0.0062168	-0.0062058	0.0022849
H. laietanus	IPS1844	-0.0023479	-0.0062867	-0.0189979	-0.0290395	0.0286423	0.0112609	-0.0017843	0.0023857	-0.0004021

SOM References

Alba, D.M., Moyà-Solà, S., 2012. On the identity of a hominoid male upper canine from the Vallès-Penedès Basin figured by Pickford (2012). Estud. Geol. 68, 149–153.

Alba, D.M., Fortuny, J., Pérez de los Ríos, M., Zanolli, C., Almécija, S., Casanovas-Vilar, I., Robles, J.M., Moyà-Solà, S., 2013. New dental remains of *Anoiapithecus* and the first appearance datum of hominoids in the Iberian Peninsula. J. Hum. Evol. 65, 573–584.

Alba, D.M., Fortuny, J., Robles, J.M., Bernardini, F., Pérez de los Ríos, M., Tuniz, C., Moyà-Solà, S., Zanolli, C., 2020. A new dryopithecine mandibular fragment from the middle Miocene of Abocador de Can Mata and the taxonomic status of '*Sivapithecus*' *occidentalis* from Can Vila (Vallès-Penedès Basin, NE Iberian Peninsula). J. Hum. Evol. 145, 102790.

Benazzi, S., Panetta, D., Fornai, C., Toussaint, M., Gruppioni, G., Hublin, J.-J., 2014. Technical Note: Guidelines for the digital computation of 2D and 3D enamel thickness in hominoid teeth. Am. J. Phys. Anthropol. 153, 305–313.

Coleman, M.N., Colbert, M.W., 2007. Technical note: CT thresholding protocols for taking measurements on three-dimensional models. Am. J. Phys. Anthropol. 133, 723–725.

Dray, S., Dufour, A.-B., 2007. The ade4 package: Implementing the duality diagram for ecologists. J. Stat. Softw. 22(4), 1–20.

Fajardo, R.J., Ryan, T.M., Kappelman, J., 2002. Assessing the accuracy of high-resolution X-ray computed tomography of primate trabecular bone by comparisons with histological sections. Am. J. Phys. Anthropol. 118, 1–10.

Fortuny, J., Zanolli, C., Bernardini, F., Tuniz, C., Alba, D.M., 2021. Dryopithecine palaeobiodiversity in the Iberian Miocene revisited on the basis of molar endostructural morphology. Palaeontology 64, 531–554.

Martin, L., 1985. Significance of enamel thickness in hominoid evolution. Nature 314, 260–263.

R Core Team, 2021. R: A language and environment for statistical computing. R Foundation for Statistical Computing, Vienna.

Schlager, S., 2021. Morpho: Calculations and visualizations related to geometric morphometrics. R package version 2.9. http://cran.r-project.org/web/packages/Morpho/index.html.

Smith, T.M., Olejniczak, A.J., Martin, L.B., Reid, D.J., 2005. Variation in hominoid molar enamel thickness. J. Hum. Evol. 48, 575–592.

Smith, T.M., Olejniczak, A.J., Zermeno, J.P., Tafforeau, P., Skinner, M.M., Hoffmann, A., Radovcic, J., Toussaint, M., Kruszynski, R., Menter, C., Moggi-Cecchi, J., Glasmacher, U.A., Kullmer, O., Schrenk, F., Stringer, C., Hublin, J.-J., 2012. Variation in enamel thickness within the genus *Homo*. J. Hum. Evol. 62, 395–411.

Smith, T.M., Tafforeau, P., Pouech, J., Begun, D.R., 2019. Enamel thickness and dental development in *Rudapithecus hungaricus*. J. Hum. Evol. 136, 102649.

Spoor, C.F., Zonneveld, F.W., Macho, G.A., 1993. Linear measurements of cortical bone and dental enamel by computed tomography: Applications and problems. Am. J. Phys. Anthropol. 91, 469–484.

van der Made, J., Ribot, F., 1999. Additional hominoid material from the Miocene of Spain and remarks on hominoid dispersals into Europe. Contrib. Tert. Quat. Geol. 36, 25–39.

Zanolli, C., Bouchet, F., Fortuny, J., Bernardini, F., Tuniz, C., Alba, D.M., 2023. A reassessment of the distinctiveness of dryopithecine genera from the Iberian Miocene based on enamel-dentine junction geometric morphometric analyses. J. Hum. Evol. 177, 103326.